Textures in superfluid ^{3}He-A: Hydrodynamic and magnetic effects in a cylindrical pore*

Louis J. Buchholtz† and Alexander L. Fetter
Institute of Theoretical Physics, Department of Physics, Stanford University, Stanford, California 94305
(Received 9 November 1976)

Transformation of the Ginzburg-Landau free energy for superfluid ^{3}He to cylindrical polar coordinates yields the field equations and specular boundary conditions for a cylindrical geometry. Similar transformations give the particle and spin current densities. Application to ^{3}He-A near T_c in a long pore of radius R predicts various stable configurations. For $R \gg 6$ μm, $\hat{d}$ and $\hat{l}$ flare upward near the center, inducing an extra free energy per unit length that is independent of R, and an angular momentum per particle $\approx 0.782\ \rho_s^{\parallel}/\rho$. For $R \ll 6$ μm, $\hat{d}$ is uniform and $\hat{l}$ is radial, with a depaired region of radius $\approx \xi(T)$ near the center; the corresponding extra free energy per unit length is proportional to $\ln[R/\xi(T)]$, with no current or angular momentum. In a large cylinder ($R \gg 6$ μm), an applied axial field deforms $\hat{d}$ and $\hat{l}$, increasing the angular momentum up to a critical magnetic field ($\approx$20–30 G), when $\hat{d}$ and $\hat{l}$ abruptly undergo a textural transition and become radial. In contrast, an applied axial superflow in a large cylinder decreases the angular momentum.

I. INTRODUCTION

The new low-temperature properties of ^{3}He below 2.7 mK have been widely interpreted as signaling the appearance of condensed triplet p-wave Cooper pairs.[1-3] As in the more familiar metallic superconductors, the central object of study is the gap function, which must now be generalized to a symmetric 2×2 matrix $\Delta_{\alpha\beta}$ in a spin space. This property is conveniently incorporated with the representation[4] $\Delta_{\alpha\beta} = i\Delta_\mu(\sigma_\mu\sigma_2)_{\alpha\beta}$, where σ_μ denotes a Pauli matrix and repeated indices are summed from 1 to 3. The three parameters Δ_μ transform like a vector under rotation of the spin coordinate axes. Furthermore, the assumption of p-wave symmetry implies that Δ_μ is a linear function of the unit vector $\hat{k}$ that characterizes directions on the Fermi surface, giving the representation $\Delta_\mu = A_{\mu i}\hat{k}_i$. The complex 3×3 tensor $A_{\mu i}$ serves as the order parameter for superfluid ^{3}He, with the first index referring to spin quantities and the second to spatial ones.

Further progress depends on more specific assumptions, and we here consider only the vicinity near T_c, where the free-energy density may be expanded in a Ginzburg-Landau form in powers of $A_{\mu i}$. The dominant bulk terms are given by[5]

$$\begin{aligned} F_0 = &-\alpha A^*_{\mu i}A_{\mu i} + \beta_1 A^*_{\mu i}A^*_{\mu i}A_{\nu j}A_{\nu j} \\ &+ \beta_2 A^*_{\mu i}A_{\mu i}A^*_{\nu j}A_{\nu j} + \beta_3 A^*_{\mu i}A^*_{\nu i}A_{\nu j}A_{\mu j} \\ &+ \beta_4 A^*_{\mu i}A_{\nu i}A^*_{\nu j}A_{\mu j} + \beta_5 A^*_{\mu i}A^*_{\nu i}A_{\nu j}A^*_{\mu j}\ , \end{aligned} \tag{1}$$

with α and $\{\beta_i\}$ determined either phenomenologically or from a microscopic analysis.[6-8] In the weak-coupling limit, a straightforward calculation[1,3] gives $\alpha = \frac{1}{3}N(0)(1 - T/T_c)$ and $-2\beta_1 = \beta_2 = \beta_3 = \beta_4 = -\beta_5 = 7\zeta(3)(120\pi^2)^{-1}N(0)(k_BT_c)^{-2}$, with $N(0) = m^*k_F/2\pi^2\hbar^2$ the density of states of one spin population at the Fermi surface. More general theories yield modified values, but the frequently encountered combinations $\beta_1+\beta_3 \equiv \beta_{13}$ and $\beta_2+\beta_4+\beta_5 \equiv \beta_{245}$ apparently remain positive. The terms in Eq. (1) are distinguished in that the first and second indices are contracted separately, so that F_0 is invariant under separate rotations of spin or orbital coordinate axes. To choose among the resulting manifold of degenerate orientational states, it becomes necessary to include several much smaller contributions to the free-energy density; for these latter terms, it is sufficient to retain only the leading (second-order) expressions in the order parameter.

One important such contribution is the nuclear dipole interaction,[1,3,9] which introduces a "spin-orbit" coupling. In the present formalism, this effect appears as contractions between the first and second indices of A, leading to the form

$$F_D = g_D(A^*_{\mu\mu}A_{\lambda\lambda} + A^*_{\mu\lambda}A_{\lambda\mu} - \tfrac{2}{3}A^*_{\mu\lambda}A_{\mu\lambda})\ , \tag{2}$$

where $g_D \approx (\frac{1}{10}\pi)[N(0)\gamma\hbar\ln(1.13\hbar\omega_0/k_BT_c)]^2$, $|\gamma| = 2.04\times10^4$ (G sec)$^{-1}$ and $\hbar\omega_0/k_B$ is a cutoff temperature of order $\approx$0.7 K. Note that F_D remains invariant under simultaneous rotations of the spin and orbital coordinate axes.

An external magnetic field provides another contribution[1,3] to the free-energy density. Since the (paramagnetic) magnetic-susceptibility tensor decreases on entering the condensed phase, the corresponding free-energy shift is positive

$$F_Z = g_Z H_\mu A^*_{\mu i}A_{\nu i}H_\nu\ , \tag{3}$$

where $g_Z \approx [7\zeta(3)/24\pi^2]\chi_n(k_BT_c)^{-2}(1+\frac{1}{4}Z_0)^{-1}$ and χ_n is the normal-state susceptibility, including Fermi-liquid corrections. Equation (3) shows that an external field couples to the spin indices and thus eliminates the corresponding rotational degeneracy

except about $\hat{H}$.

In principle, the finite electric polarizability of the ^{3}He atoms also implies an orientational effect for an applied electric field.[10] Such behavior has been sought unsuccessfully,[11] suggesting that the coupling constant may in fact be considerably smaller than initial estimates.[12] This question remains unresolved, and electric fields will not be considered here.

The final contribution to the free-energy density, and one of great importance, arises from the possibility of slow spatial variations in the order parameter. These terms represent kinetic and elastic energy. Retaining only terms quadratic in the gradients of $A_{\mu i}$, we have[1,3,13]

$$F_K = K_1 \partial_i A^*_{\mu i} \partial_j A_{\mu j} + K_2 \partial_j A^*_{\mu i} \partial_j A_{\mu i} + K_3 \partial_j A^*_{\mu i} \partial_i A_{\mu j} \ . \tag{4}$$

In the weak-coupling limit, K_1, K_2, and K_3 are equal[14] to $\frac{1}{5}N(0)\xi_0^2$, where $\xi_0 = [7\zeta(3)/48\pi^2]^{1/2} \times (\hbar v_F/k_B T_c) \approx 120$ Å is the coherence length that characterizes the size of a Cooper pair. More generally, however, the three coefficients may differ, and we shall follow Leggett[1] in retaining the general form. As seen below, the field equations depend on the two combinations K_2 and $K_1 + K_3$, whereas the (specular) boundary conditions involve only the ratio K_3/K_2; thus, in principle, each of the three coefficients could be determined experimentally.

These various perturbations will compete, eliminating much or all of the degeneracy. The predominant effect depends on the specific situation, whose scale will be fixed by the relative magnitude of the particular coefficients. We note that $g_D \approx 10^{32}$ (erg cm^3)$^{-1}$, $g_Z \approx 10^{29}$ erg^{-2}, and that $K_i \approx 4\times10^{25}$ (erg cm)$^{-1}$; these parameters define a characteristic field strength $H^* \equiv (g_D/g_Z)^{1/2} \approx 25$ G and a characteristic length $L^* \equiv (K_2/g_D)^{1/2} \approx 6$ μm. If $H \lesssim H^*$, then the dipole energy dominates the magnetic energy, and if the order parameter varies rapidly over distances smaller than L^*, then the kinetic energy dominates the dipole energy. Finally, we define the temperature-dependent coherence length $(K_2/\alpha)^{1/2} \equiv \xi(T) = (\frac{3}{5})^{1/2} \times \xi_0(1 - T/T_c)^{-1/2}$, which is the smallest length over which to expect appreciable changes in the order parameter. Although our ξ is equal to ξ_T of Ref. 14, we shall not use their notation because the curved boundaries complicate the decomposition into transverse and longitudinal components. Instead, $\xi(T)$ here serves as a characteristic scale of length, with the anisotropy appearing in the various numerical coefficients.

The presence of spatial derivatives in the free energy implies the possibility of particle currents with density[1,14]

$$J_i = 4\hbar^{-1}\mathrm{Im}(K_1 A^*_{\mu i} \partial_j A_{\mu j} + K_2 A^*_{\mu j} \partial_i A_{\mu j} + K_3 A^*_{\mu j} \partial_j A_{\mu i}) \ . \tag{5}$$

Correspondingly, the medium supports an angular momentum density $m_3 \vec{r} \times \vec{J}$, whose volume integral represents the total angular momentum $\vec{L}$. Also, the existence of two spin populations suggests the possibility of pure spin transport without net mass transport. The flux of spin component λ in the direction i is given by[1,15]

$$J_{\lambda i} = -2\mathrm{Re}\epsilon_{\lambda\mu\nu}(K_1 A^*_{\mu i} \partial_j A_{\nu j} + K_2 A^*_{\mu j} \partial_i A_{\nu j} + K_3 A^*_{\mu j} \partial_j A_{\nu i}) \ . \tag{6}$$

The equilibrium configuration for $A_{\mu i}$ minimizes the total integrated free energy, subject to specific boundary conditions. In general, this procedure leads to coupled, second-order, nonlinear, partial differential equations for the nine complex elements $A_{\mu i}$. Even in a bulk uniform medium, the exact problem becomes very complicated, and the presence of (generally curved) boundaries renders an exact treatment impracticable. In this case, it becomes essential to choose a coordinate system that reflects the geometry of the problem. Indeed, the various possible textures turn out to have free energies that differ by only small amounts, so that consistent application of the correct boundary conditions is crucial. Moreover, the characteristics imposed by the boundaries affect the global configuration far beyond a local boundary layer of thickness $\approx \xi(T)$. Thus states with nearly equal free energy can have very different currents or total angular momenta.

For these reasons, we have found it convenient to use a general tensor formalism in studying the textures of superfluid ^{3}He.[16] This approach has several advantages. First, it enables us to express interesting physical quantities, like the free energy and currents, in any particular coordinate system. Although such a transformation can be carried out directly, standard tensor analysis makes the process straightforward and purely mechanical. Second, the variational basis permits us to avoid the lengthy transformation of the field equations. Instead, the scalar character of the free energy automatically provides the correct second-order differential equations for the tensor order parameter. Third, the specular boundary conditions for the "transverse" components can be interpreted as "natural" ones[17] that ensure the vanishing of the relevant surface terms in any coordinates; this property readily leads to explicit expressions for the surface conditions. Finally, the tensor formalism clearly distinguishes between general properties and those valid in particular coordinates.

As a concrete example, we here investigate the textures of ^{3}He-A in an infinite cylinder of radius R. Section II introduces the cylindrical basis, which serves to transform the free energy and transport currents. The equilibrium textures are considered in Sec. III, and Sec. IV includes the effect of an axial magnetic field or axial superflow. Throughout this paper, all quantities are given explicitly in cylindrical coordinates, and the general tensor formalism is relegated to the Appendix.

II. INTRODUCTION OF CYLINDRICAL BASIS

The first step in transforming to curvilinear coordinates is the definition of the (familiar) unit coordinate vectors

$$\hat{e}_i = \{\hat{r}, \hat{\phi}, \hat{z}\} = \{\hat{x}\cos\phi + \hat{y}\sin\phi, -\hat{x}\sin\phi + \hat{y}\cos\phi, \hat{z}\} ,$$

where the last form relates $\hat{e}_i$ to the Cartesian basis. As in other common examples of vector or tensor fields (for example, electrodynamics[18] or hydrodynamics[19]), we consider only the usual physical components of the tensor $\underline{A}$, defined by $A_{\mu i} \equiv \hat{e}_\mu^T \underline{A} \hat{e}_i$, where first and second indices continue to represent the spin and orbital quantities, and μ and i denote the set $\{r, \phi, z\}$. To be very explicit, we have

$$A_{rr} = A_{xx}\cos^2\phi + (A_{xy} + A_{yx})\cos\phi\sin\phi + A_{yy}\sin^2\phi$$

or, alternatively,

$$A_{xx} = A_{rr}\cos^2\phi - (A_{r\phi} + A_{\phi r})\cos\phi\sin\phi + A_{\phi\phi}\sin^2\phi .$$

Note that all elements of $A_{\mu i}$ have the dimensions of energy; in general, they differ from the more abstract but less familiar covariant and contravariant components common in tensor analysis.[18,20-22]

In this orthogonal basis, contributions to the free-energy density that have no derivatives are unchanged, with $A^*_{\mu i} A_{\mu i}$, for example, representing the sum of nine terms $|A_{rr}|^2 + |A_{r\phi}|^2 + \cdots$. Terms containing derivatives are affected, however, as seen by transforming $\partial_x A_{xx}$ to cylindrical coordinates. We shall use a comma to denote differentiation, including an additional factor r^{-1} in the azimuthal direction[21]:

$$A_{\mu i,j} \equiv \left\{ \frac{\partial A_{\mu i}}{\partial r} , \frac{1}{r}\frac{\partial A_{\mu i}}{\partial \phi} , \frac{\partial A_{\mu i}}{\partial z} \right\} . \tag{7}$$

A lengthy calculation starting from Eq. (4) (see Appendix) eventually yields the kinetic energy density

$$\begin{aligned} F_K = {} & K_1 A^*_{i j,j} A_{i k,k} + K_2 A^*_{i j,k} A_{i j,k} + K_3 A^*_{i j,k} A_{i k,j} \\ & + 2r^{-1}\mathrm{Re}[K_1(A^*_{r\phi}A_{\phi j,j} - A^*_{\phi\phi}A_{rj,j} + A^*_{ir}A_{ij,j}) + K_3(A^*_{rj}A_{\phi\phi,j} - A^*_{\phi j}A_{r\phi,j} + A^*_{ir}A_{i\phi,\phi} - A^*_{i\phi}A_{i\phi,r}) \\ & \quad + K_2(A^*_{rj}A_{\phi j,\phi} - A^*_{\phi j}A_{rj,\phi} + A^*_{ir}A_{i\phi,\phi} - A^*_{i\phi}A_{ir,\phi})] \\ & + r^{-2}\{(K_1 + K_3)[|A_{r\phi}|^2 + |A_{\phi\phi}|^2 + A^*_{ir}A_{ir} + 2\mathrm{Re}(A^*_{r\phi}A_{\phi r} - A^*_{rr}A_{\phi\phi})] \\ & \quad + K_2[A^*_{rj}A_{rj} + A^*_{\phi j}A_{\phi j} + A^*_{ir}A_{ir} + A^*_{i\phi}A_{i\phi} + 4\mathrm{Re}(A^*_{r\phi}A_{\phi r} - A^*_{rr}A_{\phi\phi})]\} , \end{aligned} \tag{8}$$

where repeated dummy indices are summed over $\{r, \phi, z\}$. A combination of Eqs. (1)–(3), and (8) provides the total free-energy density, whose integral must be stationary under general variations of $A_{\mu i}$. The corresponding Euler-Lagrange equations serve only a few purposes and will be omitted here. The Appendix [Eq. (A7)] expresses them in a covariant tensor notation, which displays the dependence on the two combinations K_2 and $(K_1 + K_3)$. For convenience, we abbreviate this last quantity as follows, $K_1 + K_3 \equiv 2\gamma K_2$, and recall that $\gamma = 1$ in the weak-coupling limit. The presence of r^{-2} centrifugal barriers in Eq. (8) identifies the polar axis as a singular line, and almost all solutions will reflect this character.

Transformation of the particle and spin currents proceeds analogously from Eqs. (5) and (6), and we find

$$\begin{aligned} J_i = {} & 4\hbar^{-1}\mathrm{Im}\{(K_1 A^*_{\mu i}A_{\mu j,j} + K_3 A^*_{\mu j}A_{\mu i,j} + K_2 A^*_{\mu j}A_{\mu j,i}) \\ & + r^{-1}[K_1(A^*_{\mu i}A_{\mu r} + A^*_{\phi i}A_{r\phi} - A^*_{ri}A_{\phi\phi}) + K_3(A^*_{\phi\phi}A_{ri} - A^*_{r\phi}A_{\phi i} - \delta_{ir}A^*_{\mu\phi}A_{\mu\phi} + \delta_{i\phi}A^*_{\mu\phi}A_{\mu r}) \\ & \quad + K_2 2\delta_{i\phi}(A^*_{\phi j}A_{rj} + A^*_{\mu\phi}A_{\mu r})]\} . \end{aligned} \tag{9}$$

$$\begin{aligned} J_{\lambda i} = {} & -2\epsilon_{\lambda\mu\nu}\mathrm{Re}\{(K_1 A^*_{\mu i}A_{\nu j,j} + K_3 A^*_{\mu j}A_{\nu i,j} + K_2 A^*_{\mu j}A_{\nu j,i}) \\ & + r^{-1}[K_1(A^*_{\mu i}A_{\nu r} - \delta_{\nu r}A^*_{\mu i}A_{\phi\phi} + \delta_{\nu\phi}A^*_{\mu i}A_{r\phi}) + K_3(-\delta_{\nu r}A^*_{\mu\phi}A_{\phi i} + \delta_{\nu\phi}A^*_{\mu\phi}A_{ri} - \delta_{ir}A^*_{\mu\phi}A_{\nu\phi} + \delta_{i\phi}A^*_{\mu\phi}A_{\nu r}) \\ & \quad + K_2\delta_{i\phi}(A^*_{\mu\phi}A_{\nu r} - A^*_{\mu r}A_{\nu\phi} - \delta_{\nu r}A^*_{\mu j}A_{\phi j} + \delta_{\nu\phi}A^*_{\mu j}A_{rj})]\} . \end{aligned} \tag{10}$$

As expected from physical considerations, the particle current may be proved solenoidal for any order parameter that satisfies the field equations; a general discussion may be found in the Appendix. On the other hand, the spin transport current need not be solenoidal owing to the internal Josephson effect.[15]

Ambegaokar, de Gennes, and Rainer[14] have discussed the boundary conditions for a plane surface in great detail. If $\hat{z}$ is the unit vector normal to the plane, they conclude that $A_{\mu z}$ should vanish quite generally, but that the behavior of $A_{\mu x}$ and $A_{\mu y}$ depends on the particular model considered. Specular boundary conditions provide the simplest case, when $\partial_z A_{\mu x} = \partial_z A_{\mu y} = 0$ at the boundary. From a variational view point, these conditions are "natural"[17] in that they ensure the vanishing of the transverse surface terms, independent of the variations $\delta A_{\mu x}$ and $\delta A_{\mu y}$. As shown in the Appendix, this latter prescription is readily generalized to curved boundaries whose radius of curvature exceeds the temperature-dependent coherence length, allowing a locally flat description. When applied to a cylindrical boundary, the generalized specular conditions at $r = R$ require

$$A_{\mu r} = \frac{\partial}{\partial r} A_{\mu z} = 0; \quad K_2 \frac{\partial}{\partial r} A_{\mu\phi} = K_3 \frac{1}{R} A_{\mu\phi} . \qquad (11)$$

More physically, these generalized specular boundary conditions ensure that the normal component of the particle current vanishes at the walls. We may note that Eq. (11) differs from the specular conditions used by Barton and Moore,[23] who replaced the last relation by "curl $A_{\mu\phi}$" $\equiv r^{-1}\partial_r(rA_{\mu\phi}) = 0$. The two expressions are equivalent only for the (probably unphysical) choice $K_3 = -K_2$.

III. EQUILIBRIUM TEXTURES OF ^{3}He-A

The preceding analysis applies to all triplet p-wave phases. In general, the equilibrium order parameter must be determined by integrating the exact nonlinear field equations and then comparing the free energy of the various solutions. Such a procedure is formidable, and we instead specialize to the A phase, choosing physically motivated trial forms for $A_{\mu i}$. Although the resulting states no longer satisfy the exact field equations, their variational basis ensures that the error in the free energy is only of second order. To guide the choice of trial states for ^{3}He-A in a cylinder, we expect physical quantities like the energy gap and the transport currents to be axisymmetric and translationally invariant along z. Thus $A_{\mu i}$ should contain ϕ and z only as exponential phase factors, although we shall see [Eq. (21)] that certain exceptional cases occur. Also, the intricate boundary conditions and the presence of centrifugal barriers suggest that $A_{\mu i}$ will typically depend on r, and indeed, most solutions contain a central hole of radius $\approx\xi(T)$ where $A_{\mu i}$ falls to zero.

In a uniform infinite medium, the order parameter for ^{3}He-A has the form[1,3,6,24] $A_{\mu j} = \Delta_0 \hat{d}_\mu (\hat{n}_1 + i\hat{n}_2)_j$, where $\hat{n}_1 \cdot \hat{n}_2 = 0$ and $\Delta_0 = (\frac{1}{4}\alpha/\beta_{245})^{1/2}$. Here $\hat{d}$ is an axis along which the spin of the Cooper pair has zero component, and $\hat{l} \equiv \hat{n}_1 \times \hat{n}_2$ denotes the axis of the pair's orbital angular momentum. Inclusion of the dipole coupling renders the full field equations intractable, but a first-order variational calculation shows that $\hat{d} \parallel \hat{l}$ minimizes the integral of $F_0 + F_D$. To incorporate the effect of cylindrical boundaries, we assume a generalized form

$$A_{\mu j} = \exp[iS(\vec{r})]\hat{d}_\mu(\vec{r})[\Delta_1(r)\hat{n}_1(\vec{r}) + i\Delta_2(r)\hat{n}_2(\vec{r})]_j , \qquad (12)$$

where S is real, and Δ_1 and Δ_2 depend only on r. In most cases, we shall show that $\hat{n}_1 \cdot \hat{n}_2$ vanishes to a good approximation, but that Δ_1 cannot equal Δ_2 everywhere, especially near the axis of symmetry or at the boundary. Also, the various perturbations typically force $\hat{d}$ and $\hat{l}$ to assume different directions.

In principle, substitution of Eq. (12) into the total free-energy density [Eqs. (1)–(3), and (8)] could yield the various coupled Euler-Lagrange equations for the several functions. Even this restricted program is prohibitive, however, and we shall first consider only the equilibrium texture in a cylinder of radius R, with no applied magnetic field or hydrodynamic flow. Hence we shall try various physically reasonable forms for $\hat{d}$, $\hat{n}_1$, $\hat{n}_2$, and S, comparing the corresponding total free energies. A number of observations guides this selection. (a) The bulk gap $\Delta_0 = (\alpha/4\beta_{245})^{1/2}$ implies a free-energy density $F_0 = -\alpha^2/4\beta_{245}$ which is by far the largest contribution for a nonuniform configution except in a narrow temperature interval very close close to T_c when $R \lesssim \xi(T)$. This latter region, treated by Barton and Moore,[23] is not considered in the present paper. As a result, changes in the magnitude of Δ_1 or Δ_2 have the largest effect on the free energy, representing loss of condensation energy. We may estimate the spatial dependence of Δ in two cases.[3,25] Suppose a hole of radius r_0 forms near the center; the bulk energy per unit length increases by $\approx\pi r_0^2\alpha^2/4\beta_{245}$, and the centrifugal terms in the kinetic energy contribute an amount $\approx 2\pi K_2 \int_0^R r\,dr\,\Delta^2(r) r^{-2}$. Clearly, $\Delta(r)$ must vanish at the origin to ensure convergence; a simple estimate yields a kinetic energy $2\pi K_2 \Delta_0^2 \ln(R/r_0)$. Minimizing the sum with respect to r_0 yields $r_0 = (K_2/\alpha)^{1/2} = \xi(T)$, as expected. The situation near the outer walls is more complicated, for the

boundary conditions there may be satisfied in a variety of ways. One possibility is to have $\Delta(R)=0$, which ensures that $A_{\mu r}=0$ identically. An analogous estimate shows that this reduced condensation again occurs in a surface thickness of order $\xi(T)$, and that the corresponding change in the free energy is of order $RK_2\Delta_0^2/\xi$. A second possibility is to have $\hat{l}$ radial at the walls with $\Delta(R)\approx\Delta_0$, introducing a surface layer of unfavorable dipole and bending energy. A simple estimate yields a characteristic surface thickness $\approx L^*$ with an energy $RK_2\Delta_0^2/L^*$. Evidently, this second choice is preferable for $L^*\gtrsim\xi$ (namely $\alpha\gtrsim g_D$), which holds except for $T_c-T\lesssim 3\times10^{-6}$ K.

(b) If $\hat{d}$ and $\hat{l}$ vary with position, the associated kinetic energy is minimized by making their joint characteristic scale length of order R, again indicating the global effect of the walls, even for $R\gtrsim\xi(T)$. Thus states in a confined geometry need not be simple generalizations of bulk uniform ones.

(c) Even if $\Delta(R)\neq 0$, the boundary conditions still typically imply that $\Delta_1(R)\neq\Delta_2(R)$. As seen from Eq. (Ai3), this restriction introduces terms in the free-energy density of order $\beta_{13}(\Delta_1^2-\Delta_2^2)^2$ and small contributions to F_K. A variety of trial calculations has shown that the resulting surface layer for $R\ll L^{*2}/\xi(T)$ has a thickness of order $\xi(T)$, and that $|\Delta_1^2-\Delta_2^2|_R\approx\xi(T)R^{-1}\Delta_0^2$ with a shift in the total free energy of order $\xi^3R^{-1}F_0$, much smaller than other contributions. Thus the correct orientation of $\hat{d}$ and $\hat{l}$ near the walls turns out to be more important than small changes in Δ, with $\hat{l}$ being purely radial at $r=R$ to ensure that $A_{\mu r}(R)=0$. In most cases, moreover, $\hat{l}(\vec{r})$ probably remains coplanar with the symmetry axis, which eliminates any extra curvature associated with a "swirling" configuration.

The precise form of the energetically favorable state will depend on whether F_K or F_D is larger. For $R\ll L^*$, the curvature energy predominates, and we expect $\hat{d}$ and $\hat{l}$ to be as uniform as possible, consistent with the boundary conditions and the centrifugal barrier. For $R\gg L^*$, on the other hand, the dipole energy becomes most important, for it is a volume term proportional to R^2. Thus we expect $\hat{d}\,||\,\hat{l}$ almost everywhere in a large cylinder. Finally, we may note that an axial magnetic field tends to align $\hat{d}$ in the xy plane, and that an axial superflow tends to align $\hat{l}\,||\,\hat{z}$. The final texture represents a compromise between all these competing effects. Since the kinetic energy involves $\xi(T)$ and R, the system should exhibit a variety of temperature and size-dependent effects as well as magnetic and hydrodynamic alterations. Indeed, these latter perturbations may even induce transitions between topologically distinct textures (Sec. IV).

We have identified three distinct configurations as plausible candidates for the equilibrium texture of ^{3}He-A in a cylinder. In a large cylinder ($R\gg L^*$), the dipole energy predominates, aligning $\hat{d}$ and $\hat{l}$ almost everywhere. The equilibrium structure has $\hat{d}$ and $\hat{l}$ bend continuously from radial at the walls to axial at the center, with the explicit form[3,16,26]

$$A_{\mu j}=\Delta e^{i\phi}(\hat{z}\cos\theta+\hat{r}\sin\theta)_\mu \times[f(r)\hat{\phi}+i(\hat{z}\sin\theta-\hat{r}\cos\theta)]_j\ , \tag{13}$$

where $\hat{d}\cdot\hat{z}=\hat{l}\cdot\hat{z}=\cos\theta(r)$ and Δ is a constant. In addition, we have introduced a narrow surface region $r_0<r<R$, with $f(r<r_0)=1$ and $f(r>r_0)=(r/r_0)^{K_3/K_2}$ to satisfy the boundary condition (11) on $A_{\mu\phi}$ and with $\theta(r\geq r_0)=\frac{1}{2}\pi$ to satisfy the boundary conditions (11) on $A_{\mu r}$ and $A_{\mu z}$. As discussed previously, this region turns out to have a thickness $\approx\xi(T)$ and produces negligible corrections to the total free energy. Hence we may take $r_0\approx R$, and the resulting free energy per unit length (A13) becomes

$$\int d^2r F=\pi R^2(-2\alpha\Delta^2+4\beta_{245}\Delta^4) +2\pi K_2\Delta^2 I[\theta]+2\pi K_1\Delta^2\ , \tag{14a}$$

where we assume $\alpha\gg g_D$, thereby neglecting the region $T_c-T\lesssim 10^{-6}$ K. The functional $I[\theta]$ is given by

$$I[\theta]=\int_0^R r\,dr\{\theta'^2(3+2\gamma) +r^{-2}[\sin^2\theta+4(1+\gamma)(1-\cos\theta)]\} \tag{14b}$$

with $\gamma\equiv(K_1+K_3)/2K_2$ and θ' denoting $d\theta/dr$. The centrifugal barrier requires $\theta(r=0)=0$, confirming that $\hat{l}\to\hat{z}$ as $r\to 0$. In this region, the overall phase factor $e^{i\phi}$ in Eq. (13) plays an essential role, for $A_{\mu j}$ there reduces to a uniform configuration $\propto\hat{z}_\mu(\hat{y}-i\hat{x})_j$, eliminating the curvature energy near the axis and allowing the magnitude Δ to remain finite.

Remarkably, the Euler-Lagrange equation for Eq. (14b) has an exact solution[16]

$$\cot(\tfrac{1}{2}\theta)=\tfrac{1}{2}[CR/r+(\lambda-1)r/CR]\ , \tag{15}$$

where $\lambda^{-1}=(3K_2+K_1+K_3)/K_2=3+2\gamma$, and $C=1+(2-\lambda)^{1/2}$. Figure 1 shows this function for $\gamma=1$; it differs from a purely linear approximation $\theta(r)\approx\frac{1}{2}\pi r/R$ by at most 6%. Substitution of Eq. (15) in Eq. (14) yields the total free energy, and a straightforward minimization with respect to Δ^2 leads to the final expression

$$\int d^2r F=(\pi R^2/4\beta_{245})[-\alpha^2+2\alpha R^{-2}(K_2 I+K_1)]\ , \tag{16}$$

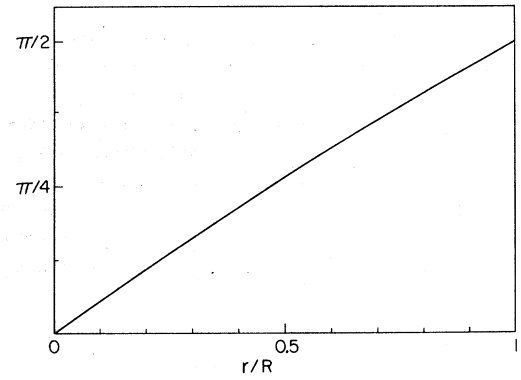

FIG. 1. Bending angle $\theta(r)$ for $\hat{l}$ and $\hat{d}$, taken from Eq. (15) with $\gamma=1$.

where

$$I=4(3+2\gamma)^{1/2}\left[(3+2\gamma)^{1/2}-\tfrac{1}{2}(5+4\gamma)^{1/2}+2(1+\gamma)\ln\left(\frac{2^{1/2}+(6+4\gamma)^{1/2}}{1+(5+4\gamma)^{1/2}}\right)\right]. \tag{17}$$

Taking $\gamma=1$ for definiteness, we find[16] $I\approx 11.4$ and a free energy per unit length $\pi R^2 F_0+24.8\pi\Delta_0^2 K_2$, where F_0 and Δ_0 are the values for bulk ^{3}He-A.

It is not difficult to show from Eq. (A14) that the trial state (13) has only an azimuthal particle current

$$J_\phi=4\Delta_0^2\hbar^{-1}[r^{-1}(2K_2+K_1+K_3)(1-\cos\theta) - K_1 d(\cos\theta)/dr], \tag{18}$$

which produces an angular momentum equivalent to that obtained by Mermin and Ho.[26] We note that rJ_ϕ is not even approximately constant owing to the spatial dependence of $\theta(r)$, and that J_ϕ vanishes smoothly at $r=0$ with the radius R acting as the characteristic scale of length. The total angular momentum per unit length can be evaluated analytically with Eq. (15) to give

$$L_z=\int d^2r\, m_3 r J_\phi = I_1\pi R^2\rho_s^{\parallel}\hbar/m_3, \tag{19a}$$

where $\rho_s^{\parallel}=16K_2(\Delta_0 m_3/\hbar)^2$ is the component of the A-phase superfluid density tensor for uniform flow parallel to $\hat{l}$ [identified from Eq. (4) or (5)], and I_1 is a numerical constant

$$I_1=\frac{1}{2}\left\{\frac{K_1}{K_2}+\left(1+\frac{K_3-K_1}{2K_2}\right)\frac{4C^2}{(\lambda-1)^2}\left[\ln\left(\frac{(1-\lambda)^2}{C^4}+\frac{2(1+\lambda)}{C^2}+1\right)-\frac{1+\lambda}{2\lambda^{1/2}}\ln\left(\frac{(\lambda-1)^2+(1-\lambda^{1/2})^2C^2}{(\lambda-1)^2+(1+\lambda^{1/2})^2C^2}\,\frac{(1+\lambda^{1/2})^2}{(1-\lambda^{1/2})^2}\right)\right]\right\}. \tag{19b}$$

For simplicity, we take $K_1=K_2=K_3$ and $\gamma=1$, to give[16]

$$L_z=0.782\pi R^2\rho_s^{\parallel}\hbar/m_3 \tag{20a}$$

or equivalently,

$$L_z N^{-1}=0.782\hbar\,\frac{\rho_s^{\parallel}}{\rho} \tag{20b}$$

per particle, quantifying a qualitative conclusion of Mermin and Ho.[26] Detailed calculation shows that the state (13) also has nonzero spin currents with components $J_{r\phi}$, $J_{\phi r}$, $J_{\phi z}$, $J_{z\phi}$; in particular, the existence of finite $J_{\phi r}$ and $J_{\phi z}$ illustrates the possibility of spin transport without associated mass transport. In concluding this discussion, we note that the spatial derivatives of $\hat{d}$ contribute substantially to the kinetic energy (14), although they do not appear explicitly in the current J. Thus any approximation that ignores spatial variations in $\hat{d}$ cannot reach numerically accurate conclusions.

The other simple limit occurs for $\xi(T)\ll R\ll L^*$, when the dipole energy is negligible relative to F_K. In this case, $\hat{d}$ becomes uncoupled from $\hat{l}$ and assumes a uniform configuration ($\hat{d}\,||\,\hat{x}$, say) to eliminate its contribution to the curvature energy. The $\hat{l}$ vector is purely radial to satisfy the boundary condition on $A_{\mu r}$, and we have an orbital disgyration[14,25] of the general form (12)

$$A_{\mu j}=\hat{x}_\mu[\Delta_1(r)\hat{\phi}+i\Delta_2(r)\hat{z}]_j = (\hat{r}\cos\phi-\hat{\phi}\sin\phi)_\mu[\Delta_1(r)\hat{\phi}+i\Delta_2(r)\hat{z}]_j. \tag{21}$$

Substitution of the last form into Eq. (8) shows that Δ_1 must vanish at the origin but that Δ_2 need not do so. Nevertheless, we take $\Delta_2(r)=\Delta_1(r)\equiv\Delta(r)$ everywhere, for this state does give a lower free energy than that with constant Δ_2. This approximation again ignores the thin surface region of thickness $\xi(T)$ at the outer walls, which has negligible effect on the free energy. The function $\Delta(r)$ obeys a nonlinear ordinary differential equation that does not scale with the single parameter r/R; instead $\Delta(r)$ falls to zero at the origin in a

characteristic length $\approx\xi(T)$. To incorporate this behavior, we have approximated $\Delta(r)$ by the form $\Delta(r/R)[(R^2+a^2)/(r^2+a)^2]^{1/2}$ treating the constants Δ and a as variational parameters. Minimizing the total integrated free energy obtained from $F_0+F_K+F_D$ shows that $\Delta\approx\Delta_0$ apart from corrections of order $(a/R)^2\ln(R/a)$, and that $a\approx(K_2/\alpha)^{1/2}=\xi(T)$, as expected. The corresponding equilibrium free energy per unit length is[16] $\pi R^2F_0+2\pi\Delta_0^2K_2\ln[R/\xi(T)]+\pi R^2g_D\Delta_0^2$, where the logarithmic factor arises from the centrifugal barrier cut off by the depairing at the origin, and the last term is the unfavorable dipole energy inherent in the different orientations of $\hat{d}$ and $\hat{l}$. Comparison with the previous calculation verifies that (21) has a lower free energy than (13) for $(R/L^*)^2+2\ln(R/\xi)\leq 24.8$; in addition, the texture (21) has neither spin nor particle currents. We may note that this state is special in that its $\hat{d}$ vector is strictly uniform, justifying an interpretation of $A_{\mu i}$ as a *vector* field with an extra Cartesian index μ.[14,23] For the other cases considered here, however, the curvature of $\hat{d}$ complicates such a treatment, as discussed in Sec. II.

A third possible state is a disgyration in both $\hat{d}$ and $\hat{l}$[14,25]

$$A_{\mu j}=\hat{r}_\mu[\Delta_1(r)\hat{\phi}+i\Delta_2(r)\hat{z}]_j\ , \tag{22}$$

where $\Delta_1(r)$ and $\Delta_2(r)$ both vanish at $r=0$ but with different power-law dependences. As in (21), however, it is convenient to ignore this difference, leaving a single variational function $\Delta(r)$. The present trial state has no important dipole energy because $\hat{d}$ and $\hat{l}$ are both radial. Using the same trial function for $\Delta(r)$ as in Eq. (21), we find $a=[(3+2\gamma)K_2/\alpha]^{1/2}\approx\sqrt{5}\,\xi(T)$ for $\gamma=1$, and the free energy per unit length

$$\approx\pi R^2F_0+2\pi\Delta_0^2K_2\{(3+2\gamma)\ln[R/(3+2\gamma)^{1/2}\xi(T)]+1+\gamma\}$$

$$\approx\pi R^2F_0+10\pi\Delta_0^2K_2[\ln(R/\xi)-0.405]$$

for $\gamma=1$. Evidently, the state (21) has lower free energy than (22) for $R^2\leq 8L^{*2}\ln(0.6R/\xi)$ so that Eq. (22) is never competitive in the relevant domain $R\ll L^*$. Nevertheless, (22) will turn out to become important in the presence of an axial magnetic field, which accounts for its inclusion here. Like Eq. (21), this latter state has neither spin nor particle currents.

For intermediate radii ($R\approx L^*$), the dipole energy is comparable with the kinetic energy incurred at the boundary and at the center. Thus the previous approximations are less compelling, for $\hat{l}$ and $\hat{d}$ will generally be coupled [unlike (21)] but unequal [unlike (13) or (22)]. Other configurations also may occur, but variational techniques may be insufficient to reveal the precise sequence of states.

To conclude this section, we shall briefly consider possible corrections to the various variational trial functions. One assumption was the orthogonality of the two unit vectors $\hat{n}_1$ and $\hat{n}_2$ in Eq. (12). It is easy to see that relaxing this constraint introduces only two new terms in the free energy

$$4\beta_{13}\Delta_1^2\Delta_2^2(\hat{n}_1\cdot\hat{n}_2)^2+2K_2(\partial_k S)\,[\Delta_1 n_{1j}\partial_k(\Delta_2 n_{2j})-\Delta_2 n_{2j}\partial_k(\Delta_1 n_{1j})]\ ,$$

where the kinetic contributions are written in Cartesian basis for simplicity. In all the cases studied so far in this work, $\Delta\hat{n}$ depends only on r whereas S depends only on ϕ, so that the gradients are orthogonal. The same conclusion also follows more tediously by direct substitution of Eq. (12) with $S=\phi$ into Eq. (8). The remaining contribution is then proportional to $(\hat{n}_1\cdot\hat{n}_2)^2$, which is clearly minimized for $\hat{n}_1\cdot\hat{n}_2=\cos\theta_{12}=0$. Thus, for the simple highly symmetric states considered here, the choice of orthogonal unit vectors is variationally correct.

The presence of axial flow changes the situation, however, for the phase factor S then acquires a dependence on r to preserve solenoidal flow (see Sec. IV B for a detailed discussion). In this case, the behavior resembles that for $\Delta_1^2\neq\Delta_2^2$ (see Sec. III), when the free-energy density acquires an extra term proportional to $\beta_{13}(\Delta_1^2-\Delta_2^2)^2$. The large value of β_{13} forces $\Delta_1^2-\Delta_2^2$ to vanish except in a thin boundary layer of thickness ξ, where $|\Delta_1^2-\Delta_2^2|$ is of order $(\xi/R)\Delta_0^2$, contributing a negligible amount $\approx(\xi/R)^3R^2F_0$ to the total free energy. Similarly, for $\hat{n}_1\cdot\hat{n}_2\neq 0$ in the presence of axial flow, the Euler-Lagrange equation for $\theta_{12}=\arccos(\hat{n}_1\cdot\hat{n}_2)$ contains dimensionless derivative terms with coefficients of order unity and a single undifferentiated term $(R/\xi)^2\sin 2\theta_{12}$. Since R/ξ is large in all cases considered here, θ_{12} remains close to $\frac{1}{2}\pi$ except possibly in thin boundary layers near the center or near the wall.

In studying the equilibrium configuration in a large cylinder, we introduced the additional approximation [Eq. (13)] that $\hat{d}$ and $\hat{l}$ were parallel. To check this step, we may define separate angles for $\hat{d}$ and $\hat{l}$, still keeping them coplanar with the symmetry axis. Thus we write $\hat{d}\cdot\hat{z}=\cos\psi$, $\hat{l}\cdot\hat{z}=\cos\theta$, and then compute the additional contributions to the total free energy per unit length from Eq. (A13). The same approximations used to obtain Eq. (14) yield the angle-dependent terms $2\pi K_2\Delta^2 I[\theta,\psi]$ where

$$I[\theta,\psi]=\int_0^1 r\,dr\{2\psi'^2(1+\gamma\cos^2\theta)+\theta'^2(1+2\gamma\sin^2\theta)$$
$$+r^{-2}[4(1+\gamma)(1-\cos\theta)+2(1+\gamma)(\sin^2\psi-\sin^2\theta)+\sin^2\theta]+(2g_DR^2/K_2)\sin^2(\theta-\psi)\}\ , \qquad (23)$$

and the integration variable is now dimensionless, measured in units of R. Note that $I[\theta,\psi]$ reduces to that in Eq. (14b) if $\theta=\psi$. The important new term is the last one, proportional to $g_DR^2/K_2 \equiv (R/L^*)^2 \gg 1$, which ensures that $|\psi-\theta|\ll 1$. To confirm this assertion, we allow ψ and θ to deviate from their common value $\theta_0(r)$ [given in Eq. (15)] by corrections $\delta\psi$ and $\delta\theta$ of order $(L^*/R)^2$, with $\delta\psi=\delta\theta=0$ at $r=0$, and $\delta\theta=0$ at $r=1$ to satisfy the boundary condition on $\hat{l}$. To first order in $(L^*/R)^2$, the Euler-Lagrange equations for $\delta\psi$ and $\delta\theta$ yield explicit formulas for $\delta\psi-\delta\theta$; these are readily proved consistent because of the explicit form of θ_0, and a little manipulation eventually gives the final expression

$$\delta\psi-\delta\theta=\frac{\sin\theta_0}{(3+2\gamma)r^2}\left(\frac{L^*}{R}\right)^2$$
$$\times[2(1+\gamma)^2(1-\cos\theta_0)$$
$$-8\gamma(1+\gamma)\cos\theta_0(1-\cos\theta_0)$$
$$-\gamma\sin^2\theta_0(2+2\gamma+3\cos\theta_0)]\ . \qquad (24)$$

Figure 2 sketches this behavior, showing that $\delta\psi-\delta\theta$ is negative near the center but becomes positive near the walls. The corresponding total free energy is altered by a term of order $(L^*/R)^2$.

IV. EFFECT OF EXTERNAL PERTURBATIONS

One of the most dramatic features of superfluid ^{3}He-A is its sensitivity to various external perturbations; for example, a magnetic field $\vec{H}$ acts to orient $\hat{d}\perp\vec{H}$ and a hydrodynamic flow $\vec{v}$ acts to orient $\hat{l}\,||\,\vec{v}$. Thus such perturbations will tend to distort the already nonuniform textures studied in Sec. III. For simplicity, we treat only the behavior for large cylinders ($R\gg L^*$), which is the case of most practical interest, and we expect that the principal changes in the order parameter (13) will represent distortions in $\hat{d}$ and $\hat{l}$, rather than changes in the magnitude of Δ. This assumption need not be correct for sufficiently large perturbations, however, which can cause a discrete transition to a topologically different texture. Unfortunately, inclusion of the various perturbations renders the Euler-Lagrange equations intractable, in large part because the presence of new dimensionless variables eliminates the simple scaled dependence on r/R. Consequently, we have resorted either to perturbation expansions or to simple sectionally smooth trial functions that may have discontinuous (but finite) first derivatives. In the latter case, the resulting total free energy then contains a variety of parameters to be determined variationally.

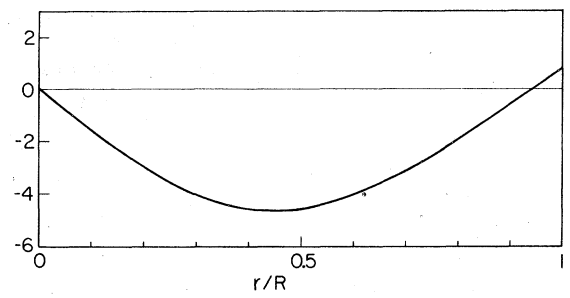

FIG. 2. The quantity $(R/L^*)^2\,[\delta\psi(r)-\delta\theta(r)]$, taken from Eq. (24) with $\gamma=1$.

A. Axial magnetic field

The perturbation of major interest is a uniform axial magnetic field $H\hat{z}$, which will tend to force $\hat{d}$ into the xy plane. The dipole energy, on the other hand, acts to keep $\hat{d}\,||\,\hat{l}$, opposing the magnetic flattening. Moreover, for states like (13), the absence of a depaired core at $r=0$ requires that $\hat{d}$ remain axial ($||\,\hat{z}$) at the origin, implying extra bending energy in a finite magnetic field. To describe this situation, we generalize the essential features of (13), allowing $\hat{d}$ and $\hat{l}$ to vary independently,

$$A_{\mu j}=e^{i\phi}\Delta(\hat{z}\cos\psi+\hat{r}\sin\psi)_\mu[\hat{\phi}+i(\hat{z}\sin\theta-\hat{r}\cos\theta)]_j\ , \qquad (25)$$

but again omitting the narrow boundary layer. This form is just that used in obtaining Eq. (23), and the finite magnetic field merely augments $I[\theta,\psi]$ by the term $(2g_ZR^2H^2/K_2)\cos^2\psi = 2h^2(R/L^*)^2\cos^2\psi$ where $h^2\equiv(H/H^*)^2$ with $H^* = (g_D/g_Z)^{1/2}\approx 25$ G. Within the class of trial states (25), it is clear that the magnetic field cannot alter the boundary condition $\psi(r=0)=0$, which arises from the term $r^{-1}\sin^2\psi$ in I. Thus we must seek other forms of the order parameter in the high-field limit [like (22)] when $\hat{d}$ is expected to be everywhere in the xy plane. Furthermore, we note that the total free energy for Eq. (25) depends on H only through the combination R^2H^2, or equivalently, the dimensionless ratio $h^2(R/L^*)^2$.

For low fields ($hR/L^*\ll 1$), it is natural to use a perturbation expansion about the approximate ground state $\psi=\theta$ given in (15). Thus, we retain $\hat{d}\,||\,\hat{l}$ and take $\psi(r)=\theta(r)=\theta_0(r)+\delta\theta(r)$ where $\delta\theta$ is a

small correction of order $(hR/L^*)^2$. The exact Euler-Lagrange equation obtained from $I[\theta,\theta]$ may be expanded to first order in the small parameter, and the explicit solution for θ_0 ultimately leads to a first integral for $\delta\theta$ of the form

$$\frac{d\delta\theta}{dr}\, r\,\frac{d\theta_0}{dr} - \delta\theta\,\frac{d}{dr}\left(r\,\frac{d\theta_0}{dr}\right) = \frac{h^2R^2}{2(3+2\gamma)L^{*2}}\,\frac{1}{r}\int_0^r dt\, t^2\,\frac{d}{dt}\cos 2\theta_0(t) \qquad (26)$$

where the right-hand side is a known function of r. This first-order ordinary differential equation for $\delta\theta(r)$ is easily solved with an integrating factor $(r\,d\theta_0/dr)^{-2}$, giving the function shown in Fig. 3. As expected physically, $\delta\theta$ is positive and vanishes at each end. The first-order field dependence of the total free energy and angular momentum (compare the treatment in Sec. III) is given by

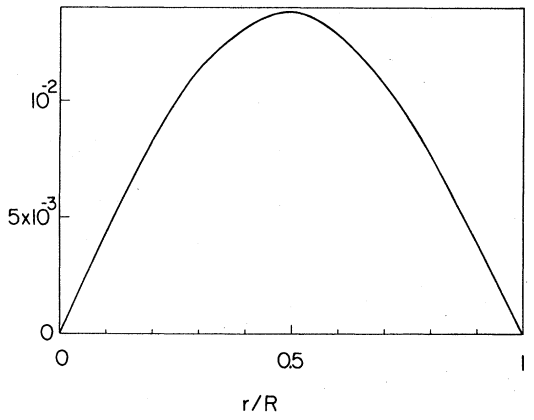

FIG. 3. First-order correction $\delta\theta(r)$ $(L^*/hR)^2$, obtained from Eq. (26) with $\gamma=1$. The dimensionless field $h=H/H^*$ is assumed small enough that $\hat{d}$ and $\hat{l}$ remain parallel.

$$\int d^2r\,F(h^2) = \pi R^2F_0 + 2\pi\Delta_0^2K_2\left(12.4 + 2(hR/L^*)^2\int_0^1 r\,dr\cos^2\theta_0\right) \approx \pi R^2F_0 + 2\pi\Delta_0^2K_2[12.4 + 0.297(hR/L^*)^2] \ , \qquad (27a)$$

$$L_z(h^2) = \pi R^2\rho_s^{\parallel}(\hbar/m_3)\left(0.782 + \int_0^1 r\,dr\sin\theta_0\delta\theta\right) \approx \pi R^2\rho_s^{\parallel}(\hbar/m_3)[0.782 + 3.27\times10^{-3}(hR/L^*)^2] \ . \qquad (27b)$$

These expressions hold even for hR/L^* of order 1, because the perturbation function $\delta\theta$ in Fig. 3 itself is of order $10^{-2}(hR/L^*)^2$. It is notable that L_z increases with increasing axial magnetic field; Eq. (27b) shows that this behavior reflects the condition $\delta\theta(r)\geq 0$.

The intermediate-field regime is more difficult, because the splitting of $\hat{d}$ and $\hat{l}$ becomes significant for $h\approx 1$. A variety of sectionally smooth variational trial states has led to the following conclusions for moderately large values of R/L^*: The free energy starts to increase quadratically in h, as in (27a), but this dependence changes to logarithmic at $h\approx 0.3$ and $R/L^*\geq 12$, when $\hat{d}$ and $\hat{l}$ start to separate appreciably. Numerical studies for $h=0.3$ and $R=20L^*$ show that the equilibrium value of $|\theta-\psi|$ never exceeds 0.01θ, but this difference rises to $\approx 0.08\theta$ for $h=1$ and grows rapidly thereafter. The corresponding angular momentum rises more smoothly for $h\gtrsim 0.3$ and then turns out to approach a field-independent value $\pi R^2\rho_s^{\parallel}\hbar/m_3$. More precisely, the expressions

$$\int d^2r\,F \approx \pi R^2F_0 + 2\pi\Delta_0^2K_2[5.55 + 9\ln(hR/L^*)] \ , \qquad (28a)$$

$$L_z \approx \pi R^2\rho_s^{\parallel}\hbar/m_3[1 - 7(L^*/hR)^2] \qquad (28b)$$

provide an approximate fit to the numerical results for $0.3\lesssim h\lesssim 1.5$, $R\gtrsim 10L^*$ and $\gamma=1$; more sophisticated trial states change these values by only a few percent. Figures 4 and 5 show the various approximations for the free energy and total angular momentum per unit length for the particular value $R=20L^*\approx 120$ μm. The different regions join smoothly, and interpolation is not difficult.

As h increases beyond ≈ 1, it eventually reaches a critical value that depends sensitively on R and temperature through $\xi(T)$. At this point, the deformed configuration (25) becomes unstable with respect to the "disgyration" texture[3,14,25] described in (22), with $\hat{d}$ and $\hat{l}$ both purely radial; the corresponding free energy is independent of H, because $\hat{d}\cdot\hat{z}=0$. As noted previously, this state (22) is topologically distinct from (25) and cannot be obtained from it through any continuous deformation. Furthermore, the absence of currents for (22) implies that L_z drops abruptly to zero above the critical field. The approximate expression (28a) shows that the transition to the state (22) occurs when

$$2.5\ln(0.45R^2/\xi^2) < 5.55 + 9\ln(HR/H^*L^*); \qquad (29)$$

at $T/T_c=0.99$, and $R=20L^*$, for example, we find the critical field $H=1.2H^*\approx 30$ G, considerably larger than the estimate in Ref. 3 owing to their omission of logarithmic factors. Figure 6 shows the approximate textural phase diagram in the hT plane for $R=20L^*$; similarly, Fig. 7 shows the

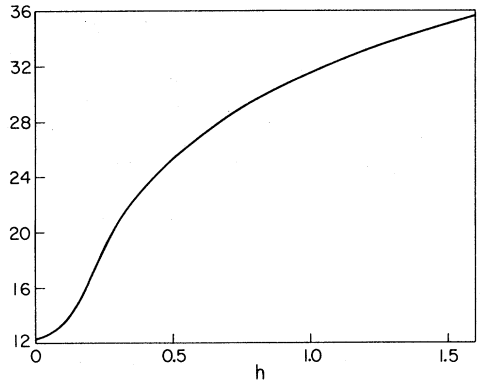

FIG. 4. Field dependence of the dimensionless free energy $(2\pi K_2\Delta_0^2)^{-1}[\int d^2r\, F(h^2) - \pi R^2 F_0]$ for the state (25) with $R = 20\,L^*$ and $\gamma = 1$.

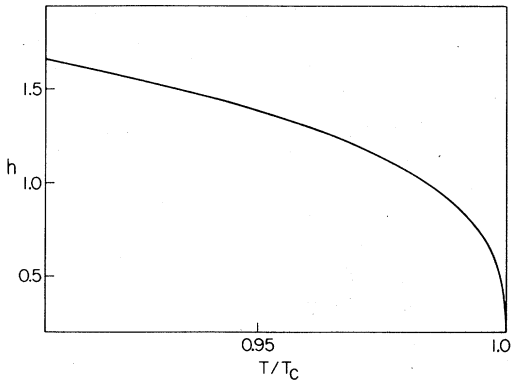

FIG. 6. Approximate textural phase diagram in the T-h plane for $R = 20L^*$. The deformed state (25) is favored below the phase boundary (at low fields) and the purely radial one (22) is favored above (at high fields).

textural phase diagram in the hR plane at $T/T_c \approx 0.963$. As is evident from Eq. (29), the disgyration structure is favored for large R and near T_c. Unfortunately, the small slope of the free energy in Fig. 4 means that small errors in the numerical values can shift the critical field considerably. Nevertheless, we hope that Eq. (29) may provide a useful scaling rule. In any case, the abrupt quenching of L_z by an axial magnetic field may be experimentally detectable, for example through the angular motion of a long suspended cylinder.[16]

In principle, the transition to the high-field limit for large R could occur through the formation of other, more complicated textures, still keeping $\hat{d}$ and $\hat{l}$ in the xy plane. One such possibility is the analog for ^{3}He-A of that considered by Brinkman *et al.*[27] for ^{3}He-B in a cylinder (Fig. 16b of Ref. 3 and Fig. 1–II of Ref. 27), with $\hat{d}$ and $\hat{l}$ everywhere parallel to eliminate the dipole energy. A detailed description of this texture involves both r and ϕ, greatly complicating the analysis. We may note that its free energy is at least comparable with that of the disgyration (22), because of the two singular lines parallel to the z axis. Like (22), this state has neither azimuthal currents nor angular momentum. Thus its macroscopic properties would not differ qualitatively from those of the disgyration, and we have not investigated it in detail.

To conclude this subsection, we remark that the clamping of $\hat{d}$ by the boundary at small fields ($h \ll 1$) implies a corresponding anisotropy in the magnetic susceptibility. More precisely, any state of the form (12) has a weak-field susceptibility[1,3] $\chi_{\mu\nu} = \chi_n \delta_{\mu\nu} - 2g_z \hat{d}_\mu \hat{d}_\nu (\Delta_1^2 + \Delta_2^2)$. Experimental studies of this effect should be feasible, and the measured quantities would represent suitable averages over the cylinder owing to the spatial variation of $\hat{d}$.

B. Axial flow

The second major perturbation of interest in a cylinder is axial flow, which is easily generated

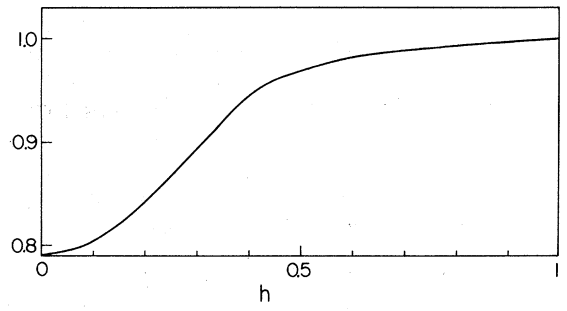

FIG. 5. Field dependence of the dimensionless angular momentum $L_z\,[\pi R^2 \rho_s^{\parallel}(\hbar/m_3)]^{-1}$ for the state (25) with $R = 20L^*$, $\gamma = 1$.

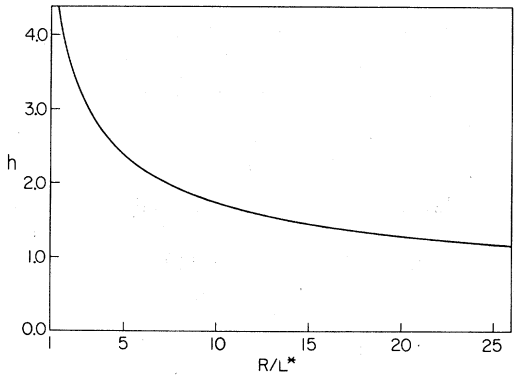

FIG. 7. Approximate textural phase diagram in the R-h plane for $T/T_c \approx 0.963$. The deformed state (25) is favored below the phase boundary (at low fields) and the purely radial one (22) is favored above (at high fields).

by differences in temperature or pressure. For simplicity, only the superfluid flow is considered, which would occur, for example, in a superleak that clamps the normal fluid.[1] In a bulk sample, the superfluid velocity $\vec{v}$ acts to orient $\hat{l}$ along the direction of flow, and a similar behavior is expected for axial flow in a cylinder. Thus $\hat{l}$ should tip toward $\hat{z}$, reducing its polar angle θ. Our principal approximation is to assume that $|\Delta|$ remains unchanged, allowing only local variations in $\hat{d}$, $\hat{n}_1$, and $\hat{n}_2$. Moreover, the small critical velocity[2,28] in ^{3}He-A ($v_c \approx 0.05$ cm sec^{-1}) ensures that the flow is a weak perturbation for $R \lesssim 0.2$ mm. Thus, a first-order expansion is sufficient.

In the presence of uniform axial flow, the order parameter acquires a phase factor[29] $\exp[iqz + iS(r)]$, where the term $S(r)$ arises from a Galilean transformation on the pairing amplitude, or more directly, to guarantee current conservation. Thus the imposition of axial flow modifies the unperturbed state of the form (A12) to

$$A_{\mu j} = e^{iqz} e^{iS(r)} e^{ip\phi} \hat{d}_\mu(r)[\vec{\Delta}_1(r) + i\vec{\Delta}_2(r)]_j . \tag{30}$$

The free energy (A13) and particle current (A14) acquire the following extra terms:

$$\begin{aligned}\delta F = {} & (K_1+K_3)\{(\Delta_{1r}S' + \Delta_{1z}q)^2 + (\Delta_{2r}S' + \Delta_{2z}q)^2 + 2S'[(\Delta_{1r}\Delta_{2r}' - \Delta_{2r}\Delta_{1r}') + (p/r)(\Delta_{1\phi}\Delta_{1r} + \Delta_{2\phi}\Delta_{2r})]\} \\ & + 2K_1 q[(\Delta_{1z}\Delta_{2r}' - \Delta_{2z}\Delta_{1r}') + (p/r)(\Delta_{1z}\Delta_{1\phi} + \Delta_{2z}\Delta_{2\phi}) + (1/r)(\Delta_{2r}\Delta_{1z} - \Delta_{1r}\Delta_{2z})] \\ & + 2K_3 q[(\Delta_{1r}\Delta_{2z}' - \Delta_{2r}\Delta_{1z}') + (p/r)(\Delta_{1\phi}\Delta_{1z} + \Delta_{2\phi}\Delta_{2z})] + K_2[(\Delta_1^2 + \Delta_2^2)(q^2 + S'^2) + 2S'(\Delta_{1i}\Delta_{2i}' - \Delta_{2i}\Delta_{1i}')] ,\end{aligned} \tag{31}$$

$$\delta J_i = (4K_2/\hbar)\{(q\delta_{iz} + S'\delta_{ir})(\Delta_1^2 + \Delta_2^2) + 2\gamma[S'(\Delta_{1i}\Delta_{1r} + \Delta_{2i}\Delta_{2r}) + q(\Delta_{1i}\Delta_{1z} + \Delta_{2i}\Delta_{2z})]\} , \tag{32}$$

where $S' \equiv dS/dr$.

The low critical velocity in bulk ^{3}He-A has the further important effect that $\hat{d}$ remains very nearly parallel to $\hat{l}$, and we therefore assume (13) for the state generated by axial flow in a wide cylinder of radius $R \gg L^*$, augmented by the additional phase factor discussed above. Substitution of Eq. (13) into Eq. (31) yields the corrections to the total free energy per unit length; we again obtain an expression of the form (14a) but with $I[\theta]$ now replaced by

$$\begin{aligned}I[\theta, S] = \int_0^1 r\,dr\{ & \theta'^2(3+2\gamma) \\ & + r^{-2}[\sin^2\theta + 4(1+\gamma)(1-\cos\theta)] \\ & + 2R^2[q^2 + S'^2 + \gamma(q\sin\theta - S'\cos\theta)^2]\} .\end{aligned} \tag{33}$$

Here the integration variable is dimensionless, measured in units of R. Since S appears only as S', its Euler-Lagrange equation is trivially solved to give

$$S'(r) = q\gamma \sin\theta\cos\theta(1+\gamma\cos^2\theta)^{-1} . \tag{34}$$

This relation is precisely that needed to eliminate the radial current density, yielding a final conserved flow, with J_ϕ given in (18) and

$$\begin{aligned}J_z &= 8K_2\Delta_0^2 q\hbar^{-1}(1+\gamma\cos^2\theta)^{-1} \\ &= \rho_s^{\parallel} m_3^{-1} v(1+\gamma\cos^2\theta)^{-1}\end{aligned} \tag{35}$$

where $\hbar q = 2m_3 v$ and $\rho_s^{\parallel}$ follows as in Eq. (19a).

The stationary properties of the free energy allow us to substitute Eq. (34) into Eq. (33), using the resulting functional to derive an Euler-Lagrange equation for θ

$$\begin{aligned}(3+2\gamma)\frac{d}{dr}(r^2\theta'^2) = {} & \frac{d}{dr}[4(1+\gamma)(1-\cos\theta) + \sin^2\theta] \\ & + 2R^2q^2r^2\frac{d}{dr}\left(\frac{1+\gamma}{1+\gamma\cos^2\theta}\right) .\end{aligned} \tag{36}$$

Although this equation cannot be integrated, we may attempt a perturbation expansion for small $(qR)^2$; just as in obtaining Eq. (26), we assume $\theta = \theta_0 + \delta\theta$ and find

$$\begin{aligned}\frac{d\delta\theta}{dr} r\frac{d\theta_0}{dr} - \delta\theta\frac{d}{dr}\left(r\frac{d\theta_0}{dr}\right) & \\ = \frac{(qR)^2}{(3+2\gamma)r}\int_0^r t^2\,dt\,\frac{d}{dt}\left(\frac{1+\gamma}{1+\gamma\cos^2\theta_0}\right) .\end{aligned} \tag{37}$$

The same integrating factor $(r d\theta_0/dr)^{-2}$ then provides an explicit expression for $\delta\theta(r)$, which, as expected, is *negative* and vanishes at $r=0$ and $r=1$. Numerical analysis shows that $|\delta\theta| \lesssim 10^{-2} \times (qR)^2$, verifying our previous assertion that this first-order description holds for $R \lesssim 5\hbar/2m_3 v_c \approx 0.2$ mm. The function $\delta\theta(r)$ is displayed in Fig. 8. The corresponding total free energy and angular momentum per unit length are

$$\int d^2r\,F(q^2) = \pi R^2 F_0 + 2\pi K_2\Delta_0^2\left(12.4 + 2(qR)^2\int_0^1 r\,dr(1+\gamma)(1+\gamma\cos^2\theta_0)^{-1}\right) \approx \pi R^2 F_0 + 2\pi K_2\Delta_0^2[12.4 + 1.608(qR)^2] \tag{38a}$$

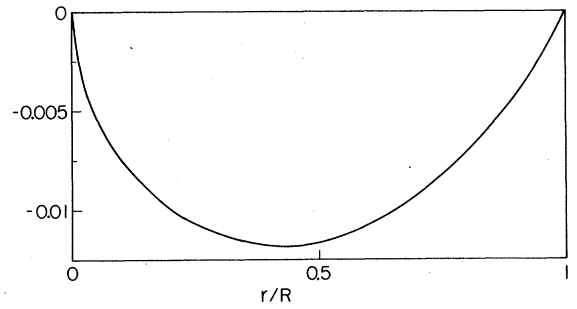

FIG. 8. First-order correction $\delta\theta(r)/2q^2R^2$ taken from Eq. (37) with $\gamma=1$. The flow is assumed sufficiently weak that $\hat{d}$ and $\hat{l}$ remain parallel.

$$L_z(q^2) = \pi R^2 \rho_s^{\parallel}(\hbar/m_3)(0.782 - 8.7\times10^{-3}q^2R^2) \ , \tag{38b}$$

where (38b) differs from (27b) only in the explicit form of $\delta\theta$. The negative sign of $\delta\theta$ causes the total angular momentum to decrease with increasing axial flow, in marked contrast to the situation for an applied axial magnetic field considered in Sec. IVA. In addition, the dependence of Eqs. (38a) and (38b) on q^2R^2 illustrates the global nature of the unperturbed state and shows that the behavior is independent of the sense of flow. Finally, the form of the corrections in (38) indicates that the texture of ^{3}He-A in a large cylinder deforms continuously in the presence of an axial flow, which differs from the predicted threshold for deformation in a channel.[29,30]

V. DISCUSSION

The present paper has analyzed the equilibrium texture of ^{3}He-A in a long circular cylinder of radius R. In the most interesting limit of large $R \gg L^*$ and $R \gg \xi(T)$, the vectors $\hat{d}$ and $\hat{l}$ are radial at the walls and turn smoothly to become axial at the center. Several authors[3,26] have analyzed such a texture, but our treatment is the first to provide quantitative values for the free energy and angular momentum that include the bending of $\hat{d}$ as well as $\hat{l}$. Moreover, it is straightforward to incorporate the effect of external perturbations, and we have obtained explicit expressions for the changes in free energy and angular momentum associated with applied axial fields or flows. Indeed, a sufficiently large field can induce a transition to a new topologically distinct texture, with $\hat{d}$ and $\hat{l}$ purely radial and no angular momentum.[3] It would be most interesting to test the prediction that an axial magnetic field increases L_z, whereas an axial superflow decreases L_z. One simple possibility is to study the angular motion of a suspended cylinder, but other configurations may be preferable. Conceivably, the sample might form metastable domains with $\hat{l}$ alternating up and down; in that case, the effect would be greatly reduced.

Our fundamental approach may be compared with that of Mermin and Ho,[26] who assume constant Δ and ignore variations in $\hat{d}$. To account for the spatial variation in the unit vectors $\hat{n}_1$ and $\hat{n}_2$, they introduce a rotation matrix that relates these orthogonal vectors at neighboring points $\vec{r}$ and $\vec{r}+d\vec{r}$. This matrix then appears explicitly in the free energy and the currents. In contrast, we start by transforming to the relevant (cylindrical) coordinate system, characterizing the order parameter at every point in space by its appropriate cylindrical components. For example, the simple requirement than $\hat{n}_1$ be azimuthal uniquely fixes its configuration everywhere. Substitution of $A_{\mu i}$ into Eqs. (8)–(10) automatically generates all contributions to the free energy and currents. In addition, our technique is sufficiently flexible to allow spatial variation of the gap function, which can be essential near the symmetry axis in certain textures like (21) and (22). As seen in Sec. IVA, omission of such effects would preclude the predicted textural transition in an axial magnetic field. Finally, the tensor formalism of the Appendix is readily extended to spherical (or other more complicated) geometries, where the topology can become even more intricate.[3,31] These matters are particularly interesting in connection with the behavior of ions in superfluid ^{3}He.

An experimental study of the NMR in cylindrical geometries would be valuable, for the nonuniform textures should yield distinctive absorption spectra. Unfortunately, the usual form of Leggett's theory[1,9] seems inadequate to discuss the behavior, when inhomogeneous textures of $\hat{d}$ and $\hat{l}$ arise from additional torques exerted by the boundaries. In this situation, the equilibrium state minimizes the total free energy, including the crucial contribution F_K; consequently, no approximation that treats the texture as uniform (and hence omits F_K) can correctly describe the first-order effect of a weak oscillatory magnetic field. The techniques introduced here should permit a generalization of Leggett's phenomenological Hamiltonian to incorporate the kinetic energy, appropriately expressed in the relevant coordinates. This question will be considered in a subsequent paper.

Another interesting extension of the present work is the consideration of vortex states, obtained from those in Secs. III and IV by adding an extra phase factor $e^{ip\phi}$, where p is an integer. Such states have additional azimuthal currents around a central region of radius $\approx\xi(T)$ where the energy gap falls to zero, and additional angular momentum. If the container rotates about its symmetry

axis with angular velocity Ω, the equilibrium configuration will minimize $\int d^2r(F - m_3\Omega n J_\phi)$. The complicated internal structure in ^{3}He-A permits a variety of states with increasing Ω, and the sequence of textures should be far more diverse than in superfluid ^{4}He, where the only freedom is the location of one or more singly quantized vortices. These theoretical questions are currently under investigation, and improved experimental capabilities should soon permit comparison with observations on rotating ^{3}He.

ACKNOWLEDGMENT

We are grateful to M. Vuorio for helpful discussions and for comments on a preliminary version of this work.

APPENDIX

In this Appendix, we introduce the general tensor formalism and apply it to the particular case of a cylindrical geometry. None of this material is required in understanding the body of the paper, although a direct derivation of the central expressions (8)–(10) would be extremely lengthy.

The principal power of tensor analysis is its ability to rewrite differential quantities in a form that holds in any coordinate system.[21] Thus an appropriate definition of the covariant derivative (denoted by a semicolon) immediately generalizes Eq. (4) to

$$F_K = K_1 A^{*i}_{\mu\,;i} A^{\mu j}_{\ \ ;j} + K_2 A^{*}_{\mu j;i} A^{\mu j;i} + K_3 A^{*j}_{\mu\ \ ;i} A^{\mu i}_{\ \ ;j} \tag{A1}$$

where $A^{\mu j;i} \equiv g^{ik} A^{\mu j}_{\ \ ;k}$. This expression transforms like a scalar under change of coordinates and reduces to Eq. (4) in a Cartesian basis. In dealing with the physical components,[18–22] discussed at the beginning of Sec. II, it is convenient to depart from the most familiar description that uses covariant and contravariant components in a coordinate basis, rather introducing an orthonormal noncoordinate basis, denoted by the addition of carets in Misner, Thorne, and Wheeler.[21] In this basis, which automatically generates the physical components of the tensor order parameter, cylindrical coordinates involve only two nonzero connection coefficients[21]

$$\Gamma^{\hat\phi}_{\hat r\hat\phi} = -\Gamma^{\hat r}_{\hat\phi\hat\phi} = r^{-1} , \tag{A2}$$

and the covariant derivatives of the tensor A are computed with the usual rules of tensor calculus. Moreover, the metric tensor reduces to the unit tensor δ_{ij}, so that the position of upper and lower indices is relevant only in terms that involve derivatives. The corresponding covariant form of the particle and spin current becomes

$$J_i = 4\hbar^{-1}\,\mathrm{Im}(K_1 A^{\mu}_{i}{}^{*} A^{j}_{\mu\,;j} + K_2 A^{\mu j *} A_{\mu j;i} + K_3 A^{\mu j *} A_{\mu i;j}) \tag{A3}$$

$$J_{\lambda i} = -2\mathrm{Re}\epsilon_{\lambda\mu\nu}(K_1 A^{\mu}_{i}{}^{*} A^{\nu j}_{\ \ ;j} + K_2 A^{\mu j *} A^{\nu}_{j;i} + K_3 A^{\mu j *} A^{\nu}_{i;j}) \tag{A4}$$

which transform like a vector and a second-rank tensor, respectively, under change of basis.

The variational principle for the free energy may be directly transcribed to the form

$$\delta \int dV F = 0 , \tag{A5}$$

where $F = F_0 + F_Z + F_D + F_K$. In performing the variation with respect to $A^{\mu j *}$, for example, the following generalization of Gauss's theorem is helpful

$$\int dV B^{i}_{\ ;i} = \int dS_i B^i . \tag{A6}$$

It holds for any vector field B^i, where dS_i is an outward surface element; in cylindrical polar coordinates, for example, $dS_{\hat r} = r\,d\phi\,dz$, $dS_{\hat\phi} = dr\,dz$, and $dS_{\hat z} = r\,dr\,d\phi$. Use of Eq. (A6) and the product rule for covariant derivatives immediately yields the nine coupled Ginzburg-Landau field equations

$$\begin{aligned} &-(\alpha + \tfrac{2}{3}g_D)A_{\mu i} + 2\beta_1 A^{*}_{\mu i} A^{\nu j} A_{\nu j} + 2\beta_2 A^{\nu j} A^{*}_{\nu j} A_{\mu i} \\ &\quad + 2\beta_3 A_{\mu j} A^{\nu j} A^{*}_{\nu i} + 2\beta_4 A_{\mu j} A^{\nu j *} A_{\nu i} + 2\beta_5 A^{*}_{\mu j} A^{\nu j} A_{\nu i} \\ &\quad + g_D(\delta_{\mu i} A^{\nu}_{\ \ \nu} + A_{i\mu}) + g_Z H_\mu H_\nu A^{\nu}_{\ \ i} - (K_1 + K_3) A^{j}_{\mu\ ;j;i} \\ &\quad - K_2 A_{\mu i}{}^{;j}_{\ \ ;j} = 0 , \end{aligned} \tag{A7}$$

which are just the Euler-Lagrange equations for the total free-energy density. As noted previously, Eq. (A7) depends on the kinetic coefficients only through the two combinations $(K_1 + K_3)$ and K_2, because the order of second covariant derivatives is irrelevant in flat space.[21] In addition, the integration by parts produces surface terms that also must vanish

$$\int dS_i (K_1 A^{k}_{\mu\ ;k}\delta^{i}_{j} + K_3 A^{i}_{\mu\ ;j} + K_2 A_{\mu j}{}^{;i}) \delta A^{\mu j *} = 0 . \tag{A8}$$

Now the basic result of Ambegaokar, de Gennes, and Rainer[14] is that

$$\hat{s}_i A^{\mu i} = 0 \tag{A9}$$

at a boundary, independent of the choice of surface conditions (specular or diffuse), where $\hat{s}$ denotes the unit vector normal to the surface. This result implies $\hat{s}_i \delta A^{\mu i *} = 0$, ensuring that the K_1 term in (A8) vanishes identically, as well as the normal components of the remaining terms. Introducing a transverse projection operator, we find the equa-

tion

$$\int dS_i A^{\mu k *}(\delta^j_k - \hat{s}^j\hat{s}_k)(K_3 A^i_{\mu\,;j} + K_2 A_{\mu\,j}{}^{;i}) = 0 \ . \quad \text{(A10)}$$

In a mathematical sense, "natural boundary conditions" are those that satisfy Eq. (A10) for arbitrary variations,[17] which here implies the single condition

$$(\delta^j_k - \hat{s}^j\hat{s}_k)(K_3 A_{\mu\,i\,;j} + K_2 A_{\mu\,j\,;i})\hat{s}^i = 0 \ . \quad \text{(A11)}$$

In Cartesian coordinates, Eqs. (A9) and (A11) precisely reproduce the specular conditions discussed above Eq. (11).[32] Thus they may be taken as an appropriate covariant generalization to arbitrary coordinates; in cylindrical coordinates, an explicit calculation using (A2) readily yields Eq. (11). As expected physically, Eqs. (A9) and (A11) also ensure that the normal component $J^i\hat{s}_i$ vanishes at the surface. It must be emphasized that these conditions are not necessarily equivalent to those of a microscopic calculation for specular reflection at a curved boundary. This more fundamental description has not yet been formulated, however, and we here restrict ourselves to the most tractable model (A9) and (A11), which we call "generalized specular" boundary conditions.

The power of the tensor formalism lies in its ability to handle general situations. One interesting example is the ease in proving the conservation of current for any state that satisfies the exact field equations (A7). Application of the covariant divergence to Eq. (A3) and use of the Euler-Lagrange equations (A7)

$$\left(\frac{\partial F}{\partial A^{\mu j *}_{\ ;i}}\right)_{;i} = \frac{\partial F}{\partial A^{\mu j *}}$$

for Eq. (A5) readily yields $J^i{}_{;i} = 0$. As mentioned in Sec. IV B, this physical requirement is the basis for inserting the phase factor $S(r)$ into Eq. (30).

In principle, it is sufficient to use the expressions in Eqs. (8)–(10) for the kinetic energy and currents in cylindrical polar coordinates. These have the advantage of applying to all phases of ^{3}He, but their general nature disguises certain special features of ^{3}He-A. For this reason, it is valuable to evaluate explicitly a few frequently occurring quantities for a state of the form

$$A_{\mu j} = e^{ip\phi}\hat{d}_\mu(r)[\vec{\Delta}_1(r) + i\vec{\Delta}_2(r)]_j$$
$$\equiv e^{ip\phi}\hat{d}_\mu(r)[\Delta_1(r)\hat{n}_1(r) + i\Delta_2(r)\hat{n}_2(r)]_j \quad \text{(A12)}$$

with $\hat{n}_1\cdot\hat{n}_2 = 0$; this includes most of those treated in this work [compare, however, Eq. (21)]. Letting primes denote d/dr and using the abbreviations $\beta_{13} = \beta_1 + \beta_3$ and $\beta_{245} = \beta_2 + \beta_4 + \beta_5$, we eventually obtain the total free-energy density

$$\begin{aligned}
F = &-(\alpha + \tfrac{2}{3}g_D)(\Delta_1^2 + \Delta_2^2) + \beta_{245}(\Delta_1^2 + \Delta_2^2)^2 + \beta_{13}(\Delta_1^2 - \Delta_2^2)^2 + 2g_D[(\hat{d}\cdot\vec{\Delta}_1)^2 + (\hat{d}\cdot\vec{\Delta}_2)^2] + g_Z(\hat{d}\cdot\vec{H})^2(\Delta_1^2 + \Delta_2^2) \\
&+ (K_1 + K_3)\{d'_\mu d'_\mu(\Delta_{1r}^2 + \Delta_{2r}^2) + (\Delta_{1r}'^2 + \Delta_{2r}'^2) + 2pr^{-1}(\Delta_{1r}\Delta'_{2\phi} - \Delta'_{1\phi}\Delta_{2r}) + (p/r)^2(\Delta_{1\phi}^2 + \Delta_{2\phi}^2) \\
&\quad + 2r^{-1}[(d_r d'_\phi - d_\phi d'_r)(\Delta_{1r}\Delta_{1\phi} + \Delta_{2r}\Delta_{2\phi}) + pr^{-1}(\Delta_{1\phi}\Delta_{2r} - \Delta_{1r}\Delta_{2\phi})] \\
&\quad + r^{-2}[(d_r^2 + d_\phi^2)(\Delta_{1\phi}^2 + \Delta_{2\phi}^2) + (\Delta_{1r}^2 + \Delta_{2r}^2)]\} \\
&+ K_2\{d'_\mu d'_\mu(\Delta_1^2 + \Delta_2^2) + \Delta'_{1i}\Delta'_{1i} + \Delta'_{2i}\Delta'_{2i} + (p/r)^2(\Delta_1^2 + \Delta_2^2) \\
&\quad + 4pr^{-2}(\Delta_{1\phi}\Delta_{2r} - \Delta_{1r}\Delta_{2\phi}) + r^{-2}[(d_r^2 + d_\phi^2)(\Delta_1^2 + \Delta_2^2) + (\Delta_{1r}^2 + \Delta_{1\phi}^2) + (\Delta_{2r}^2 + \Delta_{2\phi}^2)]\} \\
&+ K_1[2pr^{-1}(\Delta_{1\phi}\Delta_{2r} - \Delta_{2\phi}\Delta_{1r})' + r^{-1}(\Delta_{1r}^2 + \Delta_{2r}^2)'] - K_3 r^{-1}(\Delta_{1\phi}^2 + \Delta_{2\phi}^2)' \ . \qquad \text{(A13)}
\end{aligned}$$

Consideration of specific cases shows that Δ_1 and Δ_2 typically have different centrifugal barriers near the origin, implying different power-law behaviors for $r \ll \xi$ and confirming the necessity for considering two distinct functions. In a similar way, the three components of the particle current become

$$J_r = 4\hbar^{-1}\{(K_1 + K_3)[\Delta'_{1r}\Delta'_{2r} - \Delta_{2r}\Delta'_{1r} + pr^{-1}(\Delta_{1r}\Delta_{1\phi} + \Delta_{2r}\Delta_{2\phi})] + K_2(\Delta_{1j}\Delta'_{2j} - \Delta_{2j}\Delta'_{1j})\} \quad \text{(A14a)}$$

$$\begin{aligned}
J_\phi = 4\hbar^{-1}\{&K_2 r^{-1}[p(\Delta_1^2 + \Delta_2^2) + 2(\Delta_{1\phi}\Delta_{2r} - \Delta_{2\phi}\Delta_{1r})] + K_1(\Delta_{1\phi}\Delta_{2r} - \Delta_{2\phi}\Delta_{1r})' \\
&+ (K_1 + K_3)[pr^{-1}(\Delta_{1\phi}^2 + \Delta_{2\phi}^2) + r^{-1}(\Delta_{1\phi}\Delta_{2r} - \Delta_{2\phi}\Delta_{1r}) + \Delta_{1r}\Delta'_{2\phi} - \Delta_{2r}\Delta'_{1\phi}]\} \qquad \text{(A14b)}
\end{aligned}$$

$$J_z = 4\hbar^{-1}\{(K_1 + K_3)[pr^{-1}(\Delta_{1\phi}\Delta_{1z} + \Delta_{2\phi}\Delta_{2z}) + (\Delta_{1r}\Delta'_{2z} - \Delta_{2r}\Delta'_{1z})] + K_1 r^{-1}[r(\Delta_{1z}\Delta_{2r} - \Delta_{2z}\Delta_{1r})]'\} \quad \text{(A14c)}$$

which were used in obtaining Eq. (18).

*Supported in part by the NSF Grant No. DMR 75-08516.
†Supported in part by the Danforth Foundation.

[1] A. J. Leggett, Rev. Mod. Phys. 47, 331 (1975).
[2] J. C. Wheatley, Rev. Mod. Phys. 47, 415 (1975).
[3] P. W. Anderson and W. F. Brinkman, in *The Helium Liquids*, edited by J. G. M. Armitage and I. E. Farquhar (Academic, London, 1975), p. 315; see, especially, Sec. VIII.
[4] R. Balian and N. R. Werthamer, Phys. Rev. 131, 1553 (1963).

[5]N. D. Mermin and G. Stare, Phys. Rev. Lett. 30, 1135 (1973).
[6]P. W. Anderson and W. F. Brinkman, Phys. Rev. Lett. 30, 1108 (1973); W. F. Brinkman and P. W. Anderson, Phys. Rev. A 8, 2732 (1973).
[7]W. F. Brinkman, J. W. Serene, and P. W. Anderson, Phys. Rev. A 10, 2386 (1974).
[8]D. Rainer and J. W. Serene, Phys. Rev. B 13, 4745 (1976).
[9]A. J. Leggett, Ann. Phys. (N.Y.) 85, 11 (1974).
[10]J. M. Delrieu, J. Phys. (Paris) Lett. 35, L189 (1974); 36, L22 (1975).
[11]W. J. Gully, C. M. Gould, R. C. Richardson, and D. M. Lee, Phys. Lett. A 55, 27 (1975).
[12]K. Maki, Phys. Lett. A 56, 101 (1976).
[13]E. I. Blount (unpublished); D. A. Dahl, Ph.D. thesis (Stanford University, 1975) (unpublished); P. Wölfle, Phys. Lett. A 47, 224 (1974); M. C. Cross, J. Low Temp. Phys. 21, 525 (1975).
[14]V. Ambegaokar, P. G. de Gennes, and D. Rainer, Phys. Rev. A 9, 2676 (1974); A 12, 245 (1975).
[15]I. Fomin and M. Vuorio, J. Low Temp. Phys. 21, 271 (1975).
[16]L. J. Buchholtz and A. L. Fetter, Phys. Lett. A 58, 93 (1976).
[17]S. G. Mikhlin, *Variational Methods in Mathematical Physics* (Macmillan, New York, 1964), Sec. 17; L. V. Kantorovich and V. I. Krylov, *Approximate Methods of Higher Analysis* (Interscience, New York, 1964), Chap. IV, Sec. 3.
[18]L. D. Landau and E. M. Lifshitz, *The Classical Theory of Fields*, 3rd ed. (Pergamon, Oxford, 1971), see, especially p. 252.
[19]L. D. Landau and E. M. Lifshitz, *Fluid Mechanics* (Pergamon, London, 1959), Sec. 15.
[20]P. M. Morse and H. Feshbach, *Methods of Theoretical Physics* (McGraw-Hill, New York, 1953), Vol. 1, Sec. 1.5.
[21]C. W. Misner, K. S. Thorne, and J. A. Wheeler, *Gravitation* (Freeman, San Francisco, 1973), Chap. 8.
[22]C. S. Yih, *Fluid Mechanics* (McGraw-Hill, New York, 1969), Appendix 2.
[23]G. Barton and M. A. Moore, J. Low Temp. Phys. 21, 489 (1975).
[24]P. W. Anderson and P. Morel, Phys. Rev. 123, 1911 (1961).
[25]P. G. de Gennes, Phys. Lett. A 44, 271 (1973); in *Collective Properties of Physical Systems*, edited by B. Lundquist and S. Lundquist (Academic, New York, 1974), pp. 112–115.
[26]N. D. Mermin and T.-L. Ho, Phys. Rev. Lett. 36, 594 (1976).
[27]W. F. Brinkman, H. Smith, D. D. Osheroff, and E. I. Blount, Phys. Rev. Lett. 33, 624 (1974).
[28]R. T. Johnson, R. L. Kleinberg, R. A. Webb, and J. C. Wheatley, J. Low Temp. Phys. 18, 501 (1975).
[29]P. G. de Gennes and D. Rainer, Phys. Lett. A 46, 429 (1974).
[30]A. L. Fetter, Phys. Rev. B 14, 2801 (1976).
[31]S. Blaha, Phys. Rev. Lett. 36, 874 (1976).
[32]To be precise, the specular conditions $\partial_z A_{\mu x} = \partial_z A_{\mu y} = 0$ at the surface $z = 0$ have been inferred from Eq. (39) and Fig. 1 of Ref. 14. Furthermore, these conditions differ in principle from the alternative condition (Ref. 14) of zero surface torque on $\hat{d}$, which requires $d\hat{d}/dz = 0$ at $z = 0$; to verify this assertion, we consider the unphysical state $A_{\mu j} = \Delta e^{ikz} \hat{z}_\mu (\hat{x} + i\hat{y})_j$, which has $d\hat{d}/dz = 0$ everywhere, yet fails to satisfy the correct specular boundary conditions for nonzero k. As expected from our discussion below Eq. (11), this state also has a nonzero current j_z at the boundary.